Journal of Cluster Science (2018) 29:301–311
https://doi.org/10.1007/s10876-018-1336-z

ORIGINAL PAPER

Probing Structure, Thermochemistry, Electron Affinity and Magnetic Moment of Erbium-Doped Silicon Clusters $ErSi_n$ (n = 3–10) and Their Anions with Density Functional Theory

Yanpeng Zhang[1] · Jucai Yang[1,2] · Lin Cheng[1]

Received: 6 September 2017 / Published online: 10 January 2018

Abstract
The lowest energy structures and electronic properties of $ErSi_n$ (n = 3–10) and their anions were probed using the ABCluster global search technique combined with the PBE, TPSSh and B3LYP schemes. The lowest energy energies of neutral $ErSi_n$ (n = 3–10) can be regarded as substituting a Si atom of the lowest energy structure of Si_{n+1} with a Er atom. The additional electron effects on the geometries are very strong, resulting the lowest energy structures of $ErSi_n^-$ with $n > 6$ are different from their neutral counterparts. Starting from n = 7, the potential energy surfaces of $ErSi_n^-$ are very flat, resulting isomeric arrangements occur and functional dependence of the predicted most stable structures exist. The AEAs, VDEs and simulated PES of $ErSi_n$ (n = 3–10) are reported. Introducing Er to Si cluster can significantly improve photochemical reactivity of the cluster. The 4*f* electron of Er atom in $ErSi_4$, $ErSi_n^-$ (n = 4, 7–10) prefers to take part in bonding. The total magnetic moments of $ErSi_n$ and their anions are mainly provided by the 4*f* electrons of Er atom. The dissociation energies of Er from $ErSi_n$ and their anions were evaluated to inspect relative stability.

Keywords $ErSi_n$ · The lowest energy structure · Simulated PES · Electron affinity · Dissociation energy

Introduction

Silicon is not only a poor magnetic material due to absence of unpaired electrons, but also a poor photonic material because of its very short non-radiative lifetime and indirect band gap. However, doping lanthanide (Ln) metal atoms into Si clusters can improve their magnetic and optical properties because Ln atom not only has unpaired 4*f*-electrons, but also exhibits a number of intense and relatively narrow luminescence bands in the visible light and near infrared. Erbium as a dopant has been used in such optical fields as fiber amplifier, lasers, photomedicine and laser surgery, and upconversion luminescent material. Erbium doped Si clusters not only can make a silicon-based optical source: an electrically pumped optical amplifier, an injection laser or a LED (light emitting diode) [1], but also can have potential applications in the field of magnetism and spintronics. Knowledge of the ground and low-lying electronic states of neutral and anionic Er-doped silicon clusters is very important for understanding the properties and applications of these materials. With this motivation, we have done a detailed study of structure, thermochemistry, electron affinity and magnetic moment of erbium-doped silicon clusters $ErSi_n$ (n = 3–10) and their Anions using density functional theory.

Many theoretical calculations and simulations were accomplished for Ln atom doped Si clusters including $LuSi_n$ (n = 1–12) [2, 3], $YbSi_n$ ($n \leq 13$) [4–7], $HoSi_n$ ($n \leq 20$) [8–11], $TbSi_n$ ($n \leq 13$) [12], $GdSi_n$ ($n \leq 13$) [13, 14], $EuSi_n$ ($n \leq 13$) [15, 16], $SmSi_n$ ($n \leq 10$) [17, 18], $PrSi_n$ ($n \leq 21$) [19, 20], $LaSi_n$ ($n \leq 21$) [21, 22], YSi_n ($n \leq 20$) [23], and $ScSi_n$ ($n \leq 20$) [24, 25] since the photoelectron spectroscopy (PES) of $LnSi_n^-$ (Ln = Lu, Yb, Ho,

Electronic supplementary material The online version of this article (https://doi.org/10.1007/s10876-018-1336-z) contains supplementary material, which is available to authorized users.

✉ Jucai Yang
yangjc@imut.edu.cn

[1] School of Chemical Engineering, Inner Mongolia University of Technology, and Inner Mongolia Key Laboratory of Theoretical and Computational Chemistry Simulation, Hohhot 010051, People's Republic of China

[2] School of Energy and Power Engineering, Inner Mongolia University of Technology, Hohhot 010051, People's Republic of China

Tb, Gd, Eu, Sm, Pr, Sc, and Y) was recorded to probe their electronic structures and properties [26–29]. The results of theoretical simulation and experimental observation revealed that (i) in light of the patterns of the PES, the $LnSi_n$ can be divided into three types: A, B, and AB [27]. And in light of the theoretical calculations, the 4*f*-electrons of Ln atom in A type involve scarcely in bonding, while in B type, the 4*f*-electrons participate in bonding [7, 11, 14, 18, 19]. (ii) The most stable structures of small size $LnSi_n$ cluster can be regarded as substituting a Si atom of the most stable structure of Si_{n+1} with a Ln atom. That is, substitutional structure [2, 3, 7–22]. For the negatively charged ions of A type, their ground-state structures are also substitutional structure. While for negatively charged ions of B type, their ground-state structures are different from their neutral counterparts when $n \geq 7$ [11, 14, 19]. Dissimilar transition metal atom encapsulated in Si clusters, the magnetic moment of which is quenched [26, 27], the magnetic moment of Ln atom encapsulated in Si clusters is not quenched and is approximately identical to that of the free Ln atom [9, 11, 14, 16, 30].

Recently, our research group [3, 7, 11, 16, 18, 19] evaluated the most stable structures of $SmSi_n$, $EuSi_n$, $GdSi_n$, $HoSi_n$, $YbSi_n$, and $LuSi_n$ ($n \leq 10$) and their anions, as well as their adiabatic electron affinities (AEAs) by using different density functional theory, and saw that the AEAs predicted by the PBE, TPSSh, and B3LYP are agreement with experimental ones. In this study, we focused on Er-doped Si clusters to search the lowest-energy structures of $ErSi_n$ ($n \leq 10$) and their anions, and to predict their properties such as relative stability, AEA, vertical detachment energy (VDE), simulated PES, HOMO–LUMO gap, charge transfer, and magnetic moment with the goal of understanding which type (A, B, or AB) $ErSi_n$ clusters belong to and how their properties are different from those of other Ln atom-doped silicon clusters and bare silicon clusters. Our theoretical calculations and simulations will give specific instructions for the exploration of medium-size clusters and intense motivation for experimental exploration of these significant $ErSi_n$ clusters and their negatively charged ions.

Methods

The computations were implemented using the PBE [31], TPSSh [32], and B3LYP [33, 34] methods. The basis sets employed for geometry optimization are LARGE basis sets which consists of cc-pVTZ basis set [35] for Si atoms and relativistic small-core ECP28MWB segmented valence basis sets [36] for Er atom. Analyses of frequency were carried out using the three methods to warrant that the geometries reported in this study are local minima on the potential energy surface. Because the diffuse functions are important for the negatively charged ions, the LARGE basis sets are augmented, and marked as aug-LARGE (which consists of aug-cc-pVTZ basis set [35] for Si atoms and relativistic small-core ECP28MWB segmented valence basis sets [36] augmented by diffuse functions 2pdfg with exponents 0.028 and 0.015 (p), 0.032 (d), and 0.05 (f,g) [37] for Er atom). Eventually, the calculations of single-point energy, METHOD/aug-LARGE//METHOD/LARGE (METHOD = PBE, TPSSh, and B3LYP), were carried out and used for calculations of properties such as AEA, VDE, and dissociation energies (DEs). The geometry optimizations with LARGE basis sets are justifiable in respect that the structural parameters optimized with the LARGE basis sets are identical to those optimized with aug-LARGE basis sets [18]. On the other hand, the AEAs predicted by the METHOD/aug-LARGE//METHOD/LARGE (METHOD = PBE, TPSSh, and B3LYP) are agreement with experimental data. For instance, the average absolute deviations of the PBE, TPSSh, and B3LYP from experimental data are 0.07 (for 19 AEAs of $LuSi_{6–9}$, $YbSi_{4–8,10}$, and $EuSi_{3–11}$), 0.06 (for 27 AEAs of $LuSi_{6–9}$, $YbSi_{4–8,10}$, $EuSi_{3–11}$, and $SmSi_{3–10}$), and 0.10 eV (for 27 AEAs of $LuSi_{6–9}$, $YbSi_{4–8,10}$, $EuSi_{3–11}$, and $SmSi_{3–10}$) [3, 7, 16, 18], respectively. All of the calculations were performed by means of GAUSSIAN 09 software package [38].

To search for the lowest-energy structure for the $ErSi_n$ ($n = 3–10$) and their negatively charged ions, an ABCluster global search strategy [39] combined with the Gaussian 09 program is employed to choose the initial geometries. The ABCluster uses the "artificial bee colony" (ABC) algorithm to perform the global optimization. Firstly, 100 initial isomers for $n \leq 7$ and 300 isomers for $n \geq 8$ generated by ABCluster are optimized one by one by means of the PBE scheme combined with SMALL basis sets (which consists of 6-31G basis set for Si atoms and ECP57MWB basis set [40] for Er atom) and with spin multiplicities of doublet state. Secondly, the structures with the energy differences within 0.8 eV from the lowest-energy structure from the first step are selected and reoptimized by means of the PBE functional combined with LARGE basis sets. Thirdly, the structures of PBE/LARGE with the energy value within 0.8 eV from the lowest energy structure are optimized by means of the TPSSh and B3LYP method with LARGE basis sets. In addition to the initial isomers of the ABCluster, the 'substitutional structure', which are generated from replacing each Si atom of the lowest-energy structure of Si_{n+1} with a Er atom, is also considered owing to the fact that (1) the ground states

Fig. 1 Isomers of $ErSi_n$ ($n = 3–10$) clusters and their anions (Er atoms are shown in red in the online version). The Er–Si bond distances are in Å

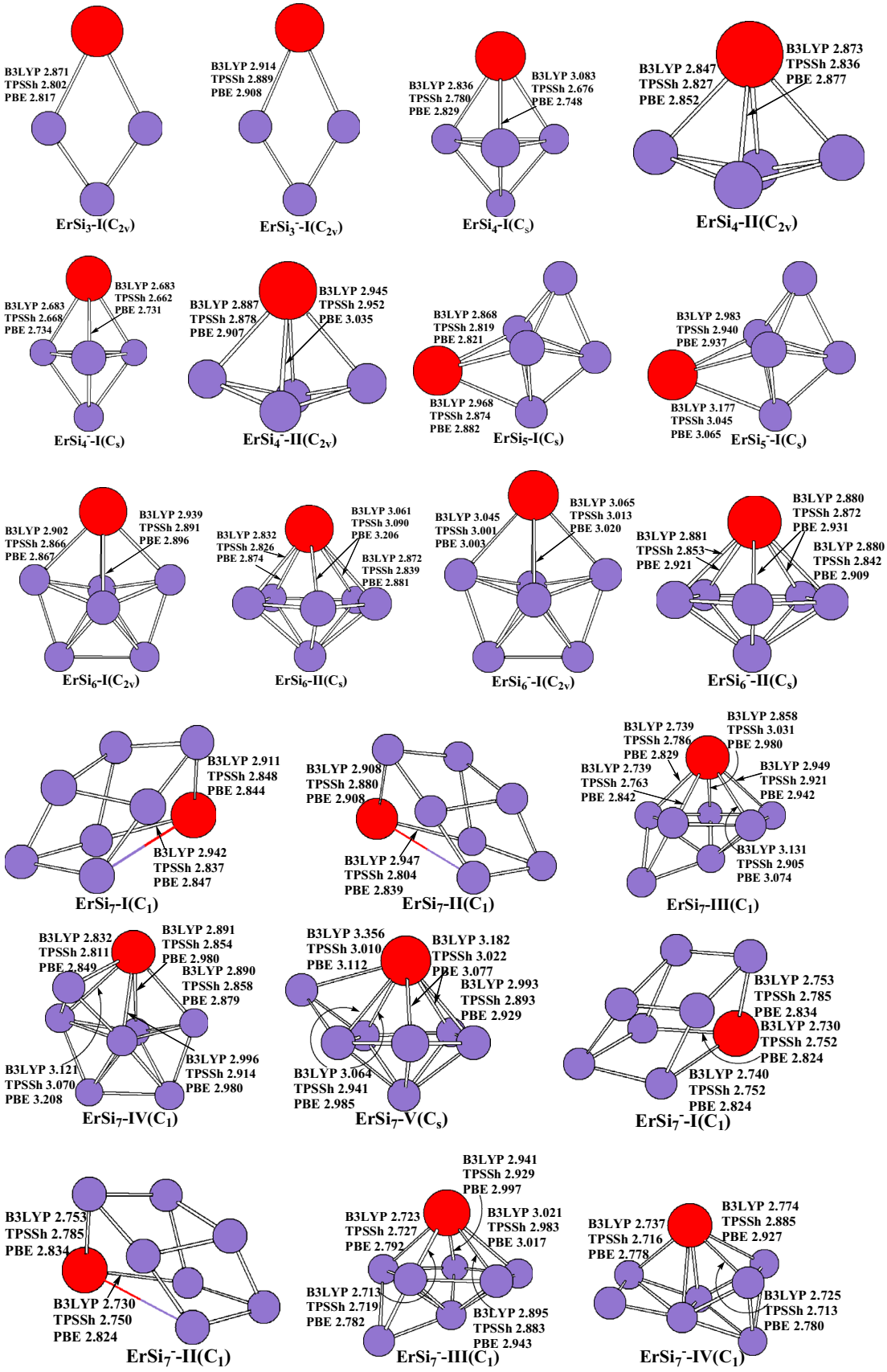
B3LYP 2.871
TPSSh 2.802
PBE 2.817
ErSi3-I(C2v)
B3LYP 2.914
TPSSh 2.889
PBE 2.908
ErSi3-(C2v)
B3LYP 2.836
TPSSh 2.780
PBE 2.829
B3LYP 3.083
TPSSh 2.676
PBE 2.748
ErSi4-I(Cs)
B3LYP 2.847
TPSSh 2.827
PBE 2.852
B3LYP 2.873
TPSSh 2.836
PBE 2.877
ErSi4-II(C2v)
B3LYP 2.683
TPSSh 2.668
PBE 2.734
B3LYP 2.683
TPSSh 2.662
PBE 2.731
ErSi4-I(Cs)
B3LYP 2.887
TPSSh 2.878
PBE 2.907
B3LYP 2.945
TPSSh 2.952
PBE 3.035
ErSi4-II(C2v)
B3LYP 2.868
TPSSh 2.819
PBE 2.821
B3LYP 2.968
TPSSh 2.874
PBE 2.882
ErSi5-I(Cs)
B3LYP 2.983
TPSSh 2.940
PBE 2.937
B3LYP 3.177
TPSSh 3.045
PBE 3.065
ErSi5-I(Cs)
B3LYP 2.902
TPSSh 2.866
PBE 2.867
B3LYP 2.939
TPSSh 2.891
PBE 2.896
ErSi6-I(C2v)
B3LYP 2.832
TPSSh 2.826
PBE 2.874
B3LYP 3.061
TPSSh 3.090
PBE 3.206
B3LYP 2.872
TPSSh 2.839
PBE 2.881
ErSi6-II(Cs)
B3LYP 3.045
TPSSh 3.001
PBE 3.003
B3LYP 3.065
TPSSh 3.013
PBE 3.020
ErSi6-I(C2v)
B3LYP 2.881
TPSSh 2.853
PBE 2.921
B3LYP 2.880
TPSSh 2.872
PBE 2.931
B3LYP 2.880
TPSSh 2.842
PBE 2.909
ErSi6-II(Cs)
B3LYP 2.911
TPSSh 2.848
PBE 2.844
B3LYP 2.942
TPSSh 2.837
PBE 2.847
ErSi7-I(C1)
B3LYP 2.908
TPSSh 2.880
PBE 2.908
B3LYP 2.947
TPSSh 2.804
PBE 2.839
ErSi7-II(C1)
B3LYP 2.739
TPSSh 2.786
PBE 2.829
B3LYP 2.739
TPSSh 2.763
PBE 2.842
B3LYP 2.858
TPSSh 3.031
PBE 2.980
B3LYP 2.949
TPSSh 2.921
PBE 2.942
B3LYP 3.131
TPSSh 2.905
PBE 3.074
ErSi7-III(C1)
B3LYP 2.832
TPSSh 2.811
PBE 2.849
B3LYP 2.891
TPSSh 2.854
PBE 2.980
B3LYP 2.890
TPSSh 2.858
PBE 2.879
B3LYP 3.121
TPSSh 3.070
PBE 3.208
B3LYP 2.996
TPSSh 2.914
PBE 2.980
ErSi7-IV(C1)
B3LYP 3.356
TPSSh 3.010
PBE 3.112
B3LYP 3.182
TPSSh 3.022
PBE 3.077
B3LYP 2.993
TPSSh 2.893
PBE 2.929
B3LYP 3.064
TPSSh 2.941
PBE 2.985
ErSi7-V(Cs)
B3LYP 2.753
TPSSh 2.785
PBE 2.834
B3LYP 2.730
TPSSh 2.752
PBE 2.824
B3LYP 2.740
TPSSh 2.752
PBE 2.824
ErSi7-I(C1)
B3LYP 2.753
TPSSh 2.785
PBE 2.834
B3LYP 2.730
TPSSh 2.750
PBE 2.824
ErSi7-II(C1)
B3LYP 2.941
TPSSh 2.929
PBE 2.997
B3LYP 2.723
TPSSh 2.727
PBE 2.792
B3LYP 3.021
TPSSh 2.983
PBE 3.017
B3LYP 2.713
TPSSh 2.719
PBE 2.782
B3LYP 2.895
TPSSh 2.883
PBE 2.943
ErSi7-III(C1)
B3LYP 2.737
TPSSh 2.716
PBE 2.778
B3LYP 2.774
TPSSh 2.885
PBE 2.927
B3LYP 2.725
TPSSh 2.713
PBE 2.780
ErSi7-IV(C1)

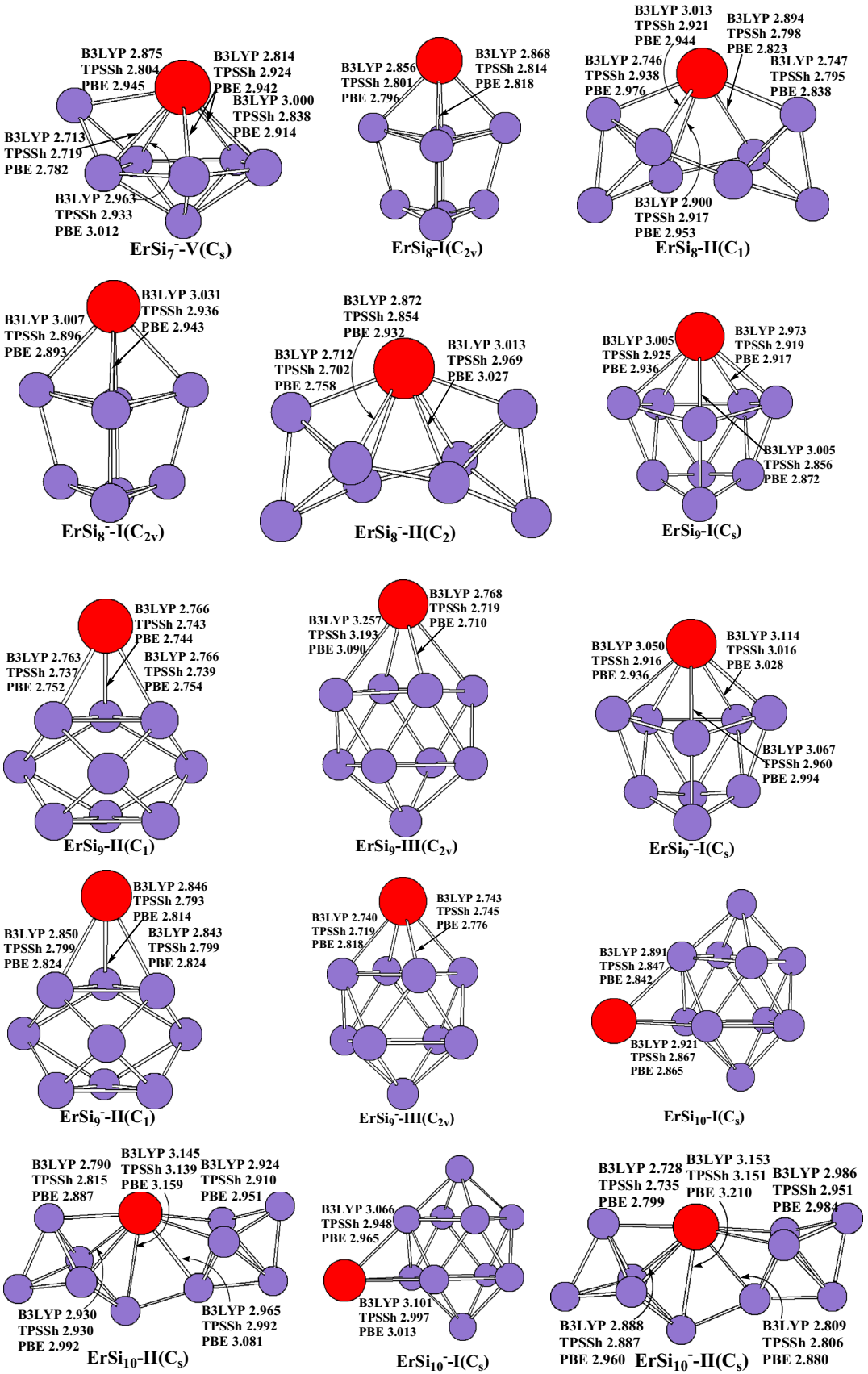

Fig. 1 continued

structure for small $LnSi_n$ (Ln = Lu, Yb, Ho, Gd, Eu, Sm, Pr, La) clusters belong to substitutional structure [2, 3, 7–22]. (2) The possibility of missing the global minimum of the potential energy surface is always exist. For small size clusters, it is can be solved by an extensive search with a global optimization scheme. However, with the size of the cluster increases, finding the true global minima becomes increasingly a challenge because of the much increased number of low-lying isomers. It is to say that it is impossible to make an "ergodic" sampling on the potential surface of large clusters by computer simulation. (3) For $LnSi_n$ clusters with n ≤ 7, the 100 initial isomers generated by the ABCluster approach include all of the substitutional structures. However starting from $n = 8$, even though 500 initial isomers generated by the ABCluster approach don't include all of the substitutional structures. In short, the selection of the initial isomer to take into account these two types is necessary to ensure the lowest-energy structure can be picked into initial isomers as much as possible. Besides, the spin multiplicity of triplet and quintuplet is taken into account for neutral $ErSi_n$, and quartet and sextuplet is considered for the negatively charged ions. The results show that the spin multiplicity of the neutral $ErSi_n$ ($n \leq 10$) is spin triplet ground state with the exception of ErSi and $ErSi_4$. The most stable structure of ErSi is spin quintuplet ground state. The triplet and quintuplet state compete with each other for the ground state of neutral $ErSi_4$. For anion $ErSi_n^-$ ($n \leq 10$), the spin multiplicity is quartet state excluded $ErSi^-$ which is sextuplet state. Despite a lot of isomers of $ErSi_n$ ($n = 3$–10) and their negatively charged ions are calculated, only several picked geometries are presented.

Results and Discussion

Structures

The geometries of $ErSi_n$ ($n = 3$–10) and their anions optimized by means of the three methods are shown in Fig. 1. The datum of spin (S) and operator S^2 is listed in Table S1 of Supporting Information. The lowest-energy structure of $ErSi_3$ and its anion is predicted to be *rhombus* with $^3B_1$ and $^4A_2$ ground state, respectively. For $ErSi_4$, at the TPSSh level, the S^2 operator analyses reveal that the spin contamination exists for the **$ErSi_4$-I** isomer of $^3A''$ electronic state because the expectation value S^2 of 2.49 is greater than 10%. The S^2 can be expanded for pure states with higher multiplicities. In quintuplet state, the most stable structure C_{2v}-symmetry **$ErSi_4$-II** of $^5B_2$ electronic state is obtained, which is more stable in energy than that of **$ErSi_4$-I** by 0.06 eV at the TPSSh level. While at the B3LYP and PBE levels, the **$ErSi_4$-I** structure is more stable in energy than that of **$ErSi_4$-II** by 0.12 and 0.06 eV, respectively. It is to say that triplet and quintuplet state compete with each other for the ground state of neutral $ErSi_4$. For negatively charged ion $ErSi_4^-$, the *distorted trigonal bipyramid* (**$ErSi_4^-$-I**) is calculated to be the lowest-energy structure with $^4A''$ ground state, which is more stable in energy than the **$ErSi_4^-$-II** of $^6B_2$ electronic state by 0.25, 0.31, and 0.28 eV at the METHOD = TPSSh, B3LYP, and PBE levels (METHOD/aug-LARGE//METHOD/LARGE), respectively. The lowest-energy structure of $ErSi_5$ and its anion is evaluated to be C_s-symmetry *face-capped trigonal bipyramid* with $^3A'$ and $^4A'$ ground state, respectively. Two isomers are reported for $ErSi_6$. The lowest-energy structure is predicted to be C_{2v}-symmetry *pentagonal bipyramid* (**$ErSi_6$-I**) of $^3A_2$ ground state, which is more stable in energy than that of **$ErSi_6$-II**, C_s-symmetry *pentagonal bipyramid* of $^3A''$ electronic state, by 0.84, 0.57, and 0.76 eV at the TPSSh, B3LYP, and PBE levels, respectively. On the other hand, the S^2 operator analysis shows that the spin contamination occurs for the **$ErSi_6$-II** isomer of triplet electronic state at the TPSSh, B3LYP and PBE levels of the theory. Calculations of quintuplet state are performed. The results show that spin contamination disappear, but the energies of quintuplet and triplet state differ little from each other at the TPSSh, B3LYP, and PBE levels. For negatively charged ion $ErSi_6^-$, at the TPSSh, and PBE levels, the **$ErSi_6^-$-I** of $^4A_2$ electronic state is more stable in energy than that of the **$ErSi_6^-$-II** of $^4A''$ electronic state by 0.17 and 0.11 eV, respectively. However at the B3LYP level, both are nearly degenerately, the **$ErSi_6^-$-I** is only less stable in energy than that of the **$ErSi_6^-$-II** by 0.05 eV. Five geometries for $ErSi_7$ are presented. The most stable structure is evaluated to be enantiomers (**$ErSi_7$-I** and **$ErSi_7$-II**). It is to say that the ground state structure of $ErSi_7$ possesses optical activity.

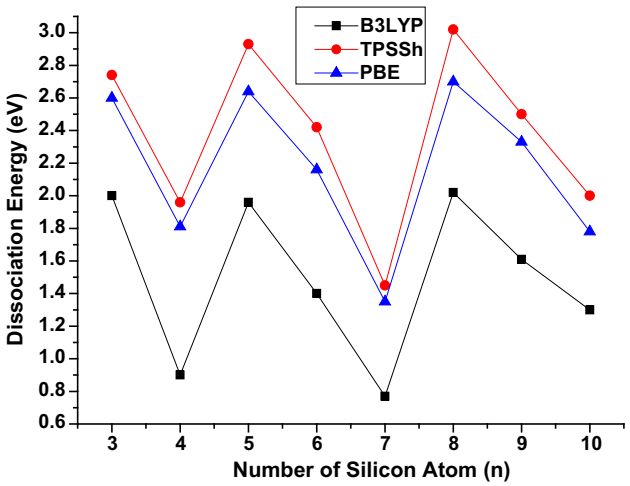

Fig. 2 Dissociation energy with ZPVE correction for the reaction $ErSi_n \rightarrow Er + Si_n$ versus the number of atoms n for $ErSi_n$ clusters

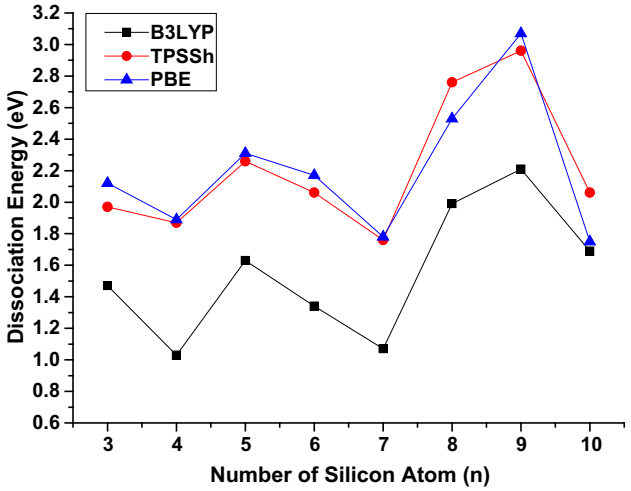

Fig. 3 Dissociation energy with ZPVE correction for the reaction $ErSi_n^- \rightarrow Er + Si_n^-$ versus the number of atoms n for $ErSi_n^-$ clusters

They can be obtained via replacing a Si atom of the most stable *distorted bicapped octahedron* of Si_8 [41, 42] with a Er atom. The second lowest-energy **ErSi$_7$-III** isomer is higher in energy than the enantiomers by 0.12, 0.23, and 0.14 eV at the TPSSh, B3LYP and PBE levels, respectively. The **ErSi$_7$-IV** isomer can be viewed as attaching a Si atom to the face of the lowest-energy structure of $ErSi_6$. Energetically, it and **ErSi$_7$-V** of $^3A'$ electronic state is much higher than that of the enantiomers at the three levels of theory. The S^2 operator analyses for **ErSi$_7$-III** and **ErSi$_7$-IV** of triplet state at the three levels, and **ErSi$_7$-V** at the TPSSh level show that the spin contamination occurs. Calculations of quintuplet state indicate that the energies of the quintuplet and triplet state, again, differ little from each other. For negatively charged ion $ErSi_7^-$, the energies of the **ErSi$_7^-$-III** and the enantiomers (**ErSi$_7^-$-I** and **ErSi$_7^-$-II**) differ little from each other. The **ErSi$_7^-$-III** structure is only more stable in energy than the enantiomers by 0.08, 0.11, and 0.04 eV at the TPSSh, B3LYP and PBE levels, respectively. It is to say that the potential energy surface of the $ErSi_7^-$ is very flat, and that many isomeric arrangements are possible, analogous to $LuSi_7^-$ [3]. The isomers **ErSi$_7^-$-IV** and **ErSi$_7^-$-V** of $^4A'$ electronic state are much higher in energy than the structure **ErSi$_7^-$-III** at the three levels of theory. For $ErSi_8$, two isomers are reported. The lowest-energy structure is predicted to be *bicapped pentagonal bipyramid* (**ErSi$_8$-I**) with $^3B_2$ ground state. The *co-apex di-trigonalbipyramind* (**ErSi$_8$-II**) of ^3A electronic state is higher in energy than that of **ErSi$_8$-I** by 0.53, 0.55 and 0.37 eV at the TPSSh, B3LYP, and PBE levels, respectively. At the same time, the spin contamination exists for the **ErSi$_8$-II** of ^3A electronic state. In quintuplet state, the energy differs little from that of triplet state at the three levels. For anion $ErSi_8^-$, at the TPSSh and B3LYP hybrid density functional levels, the *bicapped pentagonal bipyramind* (**ErSi$_8^-$-I**) of $^4B_2$ electronic state is less stable in energy than the *co-apex di-trigonalbipyramid* (**ErSi$_8^-$-II**) of ^4A electronic state by 0.19 and 0.20 eV, respectively. While at the PBE pure density functional level of theory, the **ErSi$_8^-$-I** is more stable than the **ErSi$_8^-$-II** by 0.11 eV. Three isomers for $ErSi_9$ are presented. The C_s symmetry **ErSi$_9$-I** of $^3A'$ ground state is predicted to be the most stable structure, which belongs to substitutional structure and is similar to the ground state structure of $LuSi_9$ [3]. The **ErSi$_9$-II** isomer is also substitutional structure. Energetically, it is less stable than the **ErSi$_9$-I** by 0.09, 0.20, and 0.12 eV at the TPSSh, B3LYP and PBE levels, respectively. On the other hand, the spin contamination exists for **ErSi$_9$-II**. Although the spin contamination disappears in quintuplet state, the energy of quintuplet state is above that of triplet state. The C_{2v} symmetry *bicapped antitetragonal prism* (**ErSi$_9$-III**) of $^3B_2$ electronic state is 0.23, 0.18, and 0.15 eV above the **ErSi$_9$-I** in energy at the TPSSh, B3LYP and PBE levels, respectively. For negatively charged ion $ErSi_9^-$, the energies of *tetra-capped trigonal prism* (**ErSi$_9^-$-II**) and *bicapped antitetragonal prism* (**ErSi$_9^-$-III**) differ little from each other. At the TPSSh and PBE levels, the **ErSi$_9^-$-II** is more stable than the **ErSi$_9^-$-III** by 0.06 and 0.09 eV, respectively, while less stable by 0.07 eV at the B3LYP level. The energy of **ErSi$_9^-$-I** isomer is much higher than the structures of **ErSi$_9^-$-II** and **ErSi$_9^-$-III**. For example, the **ErSi$_9^-$-I** is higher in energy than the **ErSi$_9^-$-II** by 0.50, 0.50, and 0.43 eV at the TPSSh, B3LYP, and PBE levels, respectively. For $ErSi_{10}$, two isomers are reported. The *distorted tricapped tetragonal antiprim* (**ErSi$_{10}$-I**) is predicted to be the lowest-energy structure with $^3A''$ ground state. It can be viewed as substituting a Si atom of the most stable *distorted tricapped tetragonal antiprim* of Si_{11} [42] with an Er atom. The *co-apex di-face-capped-trigonal-bipyramid* (**ErSi$_{10}$-II**) of $^3A''$ electronic state is not only higher in energy but also spin contamination. For example, it is 0.74, 0.36, and 1.03 eV above the **ErSi$_{10}$-I** at the TPSSh, B3LYP, and PBE levels, respectively. And the energies of quintuplet state differ little from those of triplet state at the three levels of theory. For anion $ErSi_{10}^-$, at the TPSSh and B3LYP hybrid density functional levels, the **ErSi$_{10}^-$-I** of $^4A''$ electronic state is more stable in energy than the **ErSi$_{10}^-$-II** of $^4A''$ electronic state by 0.33 and 0.36 eV, respectively While less stable by 0.11 eV at the PBE pure density functional level of theory.

It can be drawn from the discussion that the substitutional structures are predicted to be the lowest energy structures for neutral $ErSi_n$ (n = 3–10), analogous to other Ln (Ln = Sm, Eu, Gd, Ho, Yb, Lu) atom-doped small silicon cluster. When the neutral $ErSi_n$ obtained an electron, the charge effects of this additional electron on the

Table 1 The vertical detachment energy (VDE) and adiabatic electron affinity (AEA) with ZPVE correction for $ErSi_n$ (n = 3–10) clusters

Specie	Method	AEA	VDE	Specie	Method	AEA	VDE
$ErSi_3$	TPSSh	1.58	1.66	$ErSi_7$	TPSSh	2.17	2.38
($ErSi_3$-I ← $ErSi_3^-$-I)	B3LYP	1.61	1.72	($ErSi_7$-I ← $ErSi_7^-$-III)	B3LYP	2.07	2.39
	PBE	1.59	1.67		PBE	2.06	2.31
$ErSi_4$	TPSSh	2.06	2.31	$ErSi_8$	TPSSh	2.14	2.96
($ErSi_4$-I ← $ErSi_4^-$-I)	B3LYP	2.06	2.39	($ErSi_8$-I ← $ErSi_8^-$-II)	B3LYP	2.28	2.96
	PBE	2.01	2.34		PBE	1.98	2.85
$ErSi_5$	TPSSh	1.78	1.92	$ErSi_9$	TPSSh	2.48	2.69
($ErSi_5$-I ← $ErSi_5^-$-I)	B3LYP	1.88	2.04	($ErSi_9$-I ← $ErSi_9^-$-II)	B3LYP	2.54	2.92
	PBE	1.82	1.96		PBE	2.53	2.78
$ErSi_6$	TPSSh	1.72	1.85	$ErSi_{10}$	TPSSh	2.29	3.25
($ErSi_6$-I ← $ErSi_6^-$-I)	B3LYP	1.86	2.00	($ErSi_{10}$-I ← $ErSi_{10}^-$-II)	B3LYP	2.48	3.36
	PBE	1.80	1.94		PBE	1.96	3.23

Presented in eV

lowest energy structures are very strong. As a result, the lowest energy structures of $ErSi_n^-$ are different from those of neutral counterparts starting from $n = 7$. On the other hand, starting from $n = 7$, the potential energy surfaces of $ErSi_n^-$ are very flat, resulting isomeric arrangements occur and functional dependence of the predicted most stable structures exist.

Relative Stability

The energies of Er atom dissociated from $ErSi_n$ and their anions are calculated to examine the relative stabilities. The dissociation energies (DEs) of the lowest energy structure for $ErSi_n$ (n = 3–10) and their anions calculated at the METHOD/aug-LARGE//METHOD/LARGE (METHOD = B3LYP, TPSSh, and PBE) levels are shown in Figs. 2 and 3, respectively. So as to make easy comparisons, the DEs of $YbSi_n$, $LuSi_n$ and their anions calculated at the TPSSh level are plotted in Fig. S1 of Supporting Information. The higher the DEs, the more stable the cluster. From Figs. 2, 3 and S1 we can see that for the three methods, the variation trends of DE curves are nearly identical. The order of DEs are B3LYP < PBE < TPSSh for the neutral, and B3LYP < PBE ≈ TPSSh for the anion. Similarly to $LnSi_4$ and $LnSi_7$ (Ln = Lu, Yb) and their anions, $ErSi_4$ and $ErSi_7$ and their anions are less stable, while $ErSi_5$,$ErSi_8$, $ErSi_5^-$ and $ErSi_9^-$are more stable analogous to $YbSi_5$, $YbSi_8$, $YbSi_5^-$ and $YbSi_9^-$. The DEs of neutral $ErSi_n$ and their anions are larger than those of $YbSi_n$ and their anions, and much smaller than those of $LuSi_n$ and their anions, respectively. The reason as described in Ref. [3] is that an electron of Lu atom occupies 5*d* orbital, of which feature iseasy to deforme and polarize, leading to increasing of components of covalent bond and the largest DEs of $LuSi_n$. Although Er and Yb atoms have no 5*d* electrons, the 4*f*-electrons of Er atom in $ErSi_n$ are apt to remove to 5*d* orbitals and participate in bonding (see valence configurations below). The 4*f*-electrons of Yb atom in $YbSi_n$ participate hardly in bonding [7]. Therefore, the DEs of $YbSi_n$ and their anions are less than the DEs of $ErSi_n$ and their anions, respectively.

Electronic Property

Electron affinity is not only one of the important electronic property but also a key spectral data and vitally important for use in the chemical cycle to determine bond dissociation energies. Two different types of energy separations, AEA and VDE, are predicted. The AEA and VDE is defined as the following formulas:

$$\mathrm{AEA} = \mathrm{E(optimized\ neutral)} - \mathrm{E(optimized\ anion)}$$

$$\mathrm{VDE} = \mathrm{E(neutral\ at\ optimized\ anion\ geometry)} - \mathrm{E(optimized\ anion)}$$

The AEA and VDE calculated at the METHOD/aug-LARGE//METHOD/LARGE (METHOD = B3LYP, TPSSh, and PBE) levels are listed in Table 1. From Table 1 we can see that the AEAs and VDEs predicted by the three schemes are very close to each other. There are no experimental data for comparison. So as to make easy comparisons, the AEAs of $ErSi_n$, $YbSi_n$, and $LuSi_n$ (n = 3–10) calculated at the TPSSh level are plotted in Fig. S2, as well as experimental AEAs of $YbSi_n$. From Fig. S2 we can see that (1) the AEAs of $LuSi_n$ are larger than those of $ErSi_n$ and $YbSi_n$. The AEAs of $ErSi_3$, $ErSi_5$ and $ErSi_6$ are very close to those of $YbSi_3$, $YbSi_5$ and $YbSi_6$. The AEAs of $ErSi_{4,7-10}$ are averagely larger than those of $YbSi_{4,7-10}$ by 0.24 eV. The reason is that the Lu atom includes an unpaired *d*-electron which interacts

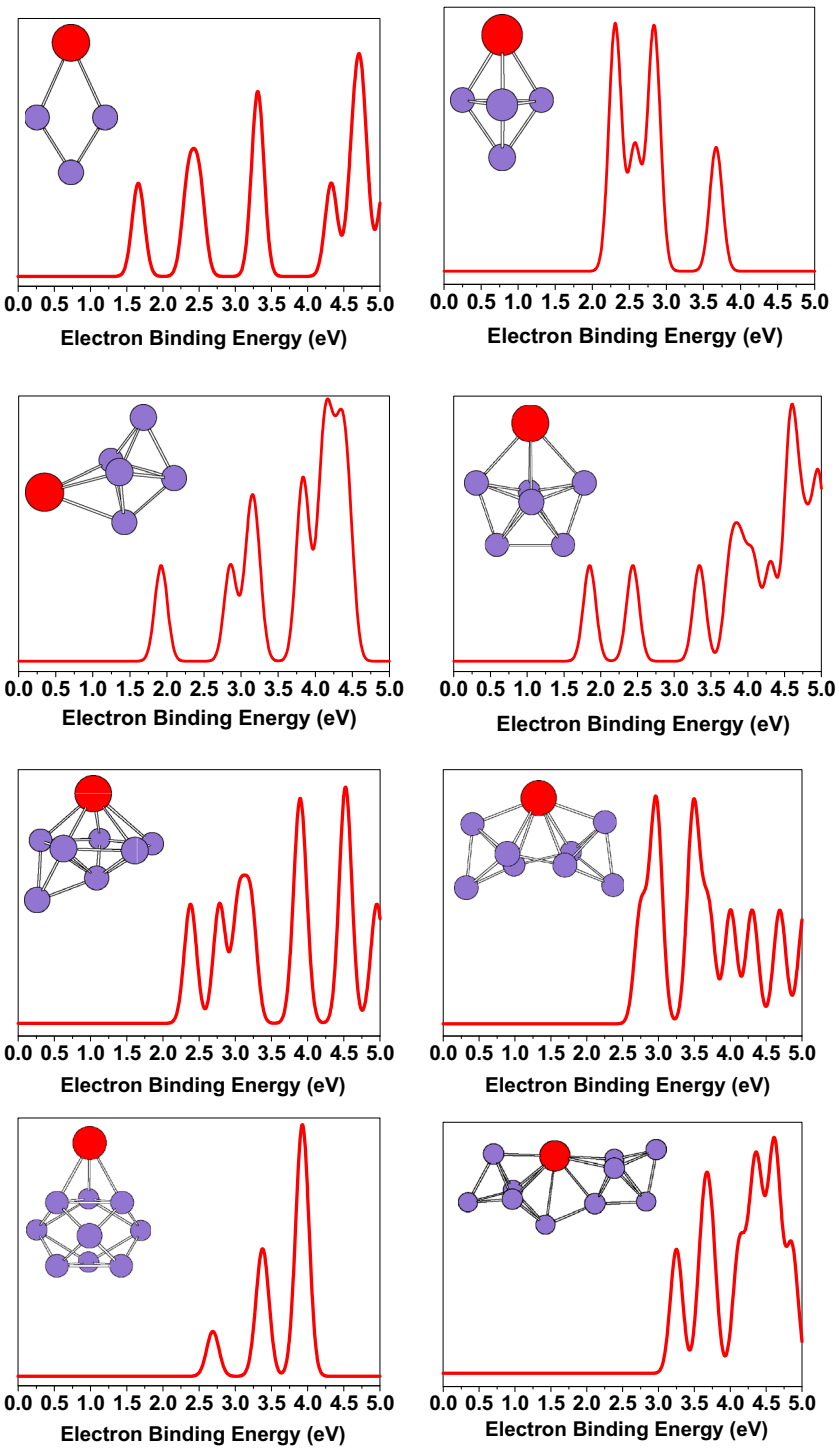

Fig. 4 Simulated photoelectron spectra for the most stable structure of $ErSi_n^-$ clusters at the TPSSh level of theory

strongly with the extra electron. The 4*f* electrons of Yb atom in anion $YbSi_n^-$ [7] and Er atom in anion $ErSi_{3,5,6}^-$ (see valence configurations below) are nearly unchanged and participate hardly in bonding, resulting AEAs of $ErSi_{3,5,6}$ are nearly identical to those to $YbSi_{3,5,6}$. While the part of 4*f* electrons of Er atom in anion $ErSi_{4,7-10}^-$ removed to 5*d* orbital (see valence configurations below) and then the 5*d* electrons participate in bonding. So The AEAs of $ErSi_{4,7-10}$ are larger than those of $YbSi_{4,7-10}$. Our calculations may give strong motivation for experimental investigations of Er-doped Si clusters and their anions.

PES as a powerful tool can probe the structure of clusters because it is susceptible to variations of the structure. Only TPSSh simulated PES is done and exhibited in Fig. 4. In the PES simulation the relative energies of the orbitals (ΔE_n) is firstly calculated by means of the formulation:

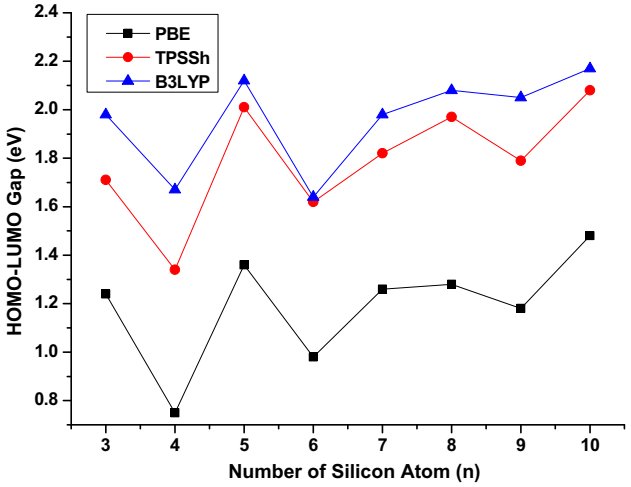

Fig. 5 HOMO-LUMO gaps (eV) of $ErSi_n$ ($n = 3$–10) calculated at the three levels

$$\Delta E_n = \Delta E_{HOMO-n} - \Delta E_{HOMO}$$

Then, the first peak related with the HOMO is placed in the VDE position, and other peaks related with deeper orbitals are moved to higher binding energies according to the data of $-\Delta E_n$. Ultimately, a Gaussian FWHM (full width at half maximum) of 0.20 eV is adopted for fit all of these peaks. As can be seen from in Fig. 4, the simulated $ErSi_3^-$ PES shows five peaks located in 1.66, 2.43, 3.31, 4.33, and 4.71 eV in the range of $\leq$ 5.0 eV, respectively. There are four major peaks for $ErSi_4^-$ located in 2.31, 2.58, 2.83 and 3.67 eV, respectively. Six major peaks located in 1.92, 2.86, 3.16, 3.84, 4.16, and 4.34 eV are observed in the simulated PES of $ErSi_5^-$. There are seven major peaks for $ErSi_6^-$ centered at 1.85, 2.43, 3.34, 3.85, 4.31, 4.60 and 4.95 eV, and six major peaks for $ErSi_7^-$ centered at 2.38, 2.78, 3.13, 3.89, 4.52, and 4.96 eV, respectively. The simulated PES of $ErSi_8^-$ exhibits five peaks centered at 2.96, 3.49, 4.00, 4.30 and 4.69 eV, respectively. Three peaks for $ErSi_9^-$ are situated at 2.69, 3.38 and 3.93 eV, respectively. The simulated PES of $ErSi_{10}^-$ in the range of $\leq$ 5.0 eV shows five peaks situated at 3.25, 3.67, 4.36, 4.61, and 4.84 eV, respectively. We think that these simulations will give strong motivation for experimental investigations of Er-doped Si clusters and their anions.

HOMO–LUMO gaps not only as a vital physical property can mirror the electronic properties but also as a key chemical property can mirror the chemical reactivity, especially for photochemical reaction. The curves of HOMO–LUMO gaps versus cluster size for the lowest energy geometries of $ErSi_n$ ($n = 3$–10) evaluated by using the three schemes are shown in Fig. 5. The HOMO–LUMO gaps of $YbSi_n$, $LuSi_n$, and Si_n predicted at the TPSSh level are shown in Fig. S3 of Supporting Information in order to make easy comparisons. From Fig. 5, we can see that the curves of HOMO–LUMO gap evaluated by the TPSSh, B3LYP, and PBE are by and large in parallel, and the orders are B3LYP > TPSSh > PBE. The reason is that the energy of HOMO and LUMO evaluated in Kohn–Sham (KS) molecular orbital approximations go through by and large the alike quantity upshift, while Hartree–Fock (HF) scheme shift the LUMO up a much higher energy levels than the HOMO up [43]. On the other hand, the pure density functional PBE method doesn't contain HF components. And the HF components of hybrid B3LYP scheme are larger than those of hybrid TPSSh method. Consequently, the orders are B3LYP > TPSSh > PBE. From Fig. S3 of Supporting Information, we can see that the curve of $ErSi_n$ parallels by and large with that of $YbSi_n$, but not that of $LuSi_n$. The HOMO–LUMO gaps of $ErSi_n$ are larger than those of $YbSi_n$, but smaller than that of Si_n with the exception of Si_3. The HOMO–LUMO gap of Si_3 is very close to that of $ErSi_3$ because the ground state structure of Si_3 is triplet state, not singlet state, leading to smaller the HOMO–LUMO gap. The smaller the HOMO–LUMO gap, the more easily the $ErSi_n$ inclines to set off photochemical reaction. Consequently, the photochemical activity of Er-doped Si_n ($n = 4$–10) clusters is stronger than that of pure Si clusters, but weaker than that of $YbSi_n$. This property can be used to manufacture novel functional materials such as optical materials, semiconductive materials, and environmental photocatalysis materials.

Moreover, the natural population analysis (NPA) charges, valence configurations, and magnetic moments for the lowest energy structure are evaluated to further understand the interaction between Er and Si clusters. The values predicted with the three schemes differ little from each other. Consequently, only TPSSh data are listed in Tables S2 and S3 of Supporting Information. Similar to other Ln in small $LnSi_n$ ($n = 3$–10) clusters [3, 7, 11, 14, 16, 18, 19], the Er atom acts as an electron donor. The valence configurations of Er in $ErSi_n$ ($n = 3$, 5–10) are $6s^{0.22-0.54}4f^{11.79-11.96}5d^{0.32-0.88}6p^{0.07-0.20}$. This indicates that the 4*f* electrons of Er in $ErSi_n$ ($n = 3$, 5–10) are hardly participate in bonding. For $ErSi_4$, the $4f^{11.53-11.58}$ valence configuration shows that a 4*f* electron prefers to take part in bonding. In the case of negatively charged ions $ErSi_n^-$ with $n = 4$, 7–10, their $4f^{11.18-11.49}$ valence configurations indicate the 4*f* electrons are also participate in bonding. It is to say that the $ErSi_n$ clusters belong to AB type. The 4*f* electrons of Er atom provide the total magnetic moments for $ErSi_n$ clusters and their anions as can be seen from Table S3.

To further understand $ErSi_n$ clusters belong to AB type, the PES of $ErSi_n^-$, $YbSi_n^-$, and $LuSi_n^-$ ($n = 4$–7) are simulated at the TPSSh level and shown in Fig. S4 of Supporting Information. According to the classification of Grubisic et al. [27], spectra of A type are distinguished by a

low electron binding energy feature. The representative is spectra of $EuSi_n^-$ (Eu: half-filled 4*f*-electrons) and $YbSi_n^-$ (Yb: full-filled 4*f*-electrons). Spectra of B type are lack of comparably low electron binding energy peaks. The representative is spectra of $GdSi_n^-$ and $LuSi_n^-$ (both have a 5*d*-electron). Some of spectra of AB resemble those of A, and others resemble those of B. In this study, we only choose $YbSi_n/YbSi_n^-$ and $LuSi_n/LuSi_n^-$ as representative for comparison. As can be seen from Fig. S4, the spectra of $ErSi_5^-$ and $ErSi_6^-$ resemble that of $YbSi_5^-$ and $YbSi_6^-$, respectively. Spectra of $ErSi_4^-$ resemble that of $LuSi_4^-$. While spectra of $ErSi_7^-$ is spectral superposition of $YbSi_7^-$ and $LuSi_7^-$.

Conclusions

The lowest energy structures and electronic properties of $ErSi_n$ ($n = 3$–10) clusters and their negatively charged ions were systematically studied using the ABCluster global search technique combined with the PBE, TPSSh and B3LYP schemes. The results revealed that the ground state is triplet electronic state for $ErSi_n$ ($n = 3$–10) excluded $ErSi_4$, for which the triplet and quintuplet state compete with each other. For anion $ErSi_n^-$ ($n = 3$–10), the spin multiplicity is quartet state. the lowest energy energies of neutral $ErSi_n$ ($n = 3$–10) are substitutional structures, similar to other Ln metal atoms-doped small silicon cluster such as $LnSi_n$ (Ln = Sm, Eu, Gd, Ho, Yb, Lu). When the neutral $ErSi_n$ gained an electron, the charge effects of this additional electron on the lowest energy structures are very strong. As a result, the lowest energy structures of $ErSi_n^-$ are different from those of neutral counterparts starting from $n = 7$. On the other hand, starting from $n = 7$, the potential energy surfaces of $ErSi_n^-$ are very flat, resulting isomeric arrangements occur and functional dependence of the predicted most stable structures exist. The DEs of neutral $ErSi_n$ and their anions are larger than those of $YbSi_n$ and their anions, and much smaller than those of $LuSi_n$ and their anions, respectively. The AEAs, VDEs and simulated PES of $ErSi_n$ ($n = 3$–10) are reported. Evaluation of HOMO–LUMO gap revealed that Er-doped Si cluster can significantly improve photochemical reactivity of the cluster. And the improved effects are weaker than those of the introducing Yb atom to Si cluster. The NPA analyses revealed that the 4*f* electron of Er atom in $ErSi_4$, $ErSi_4^-$, $ErSi_7^-$, $ErSi_8^-$, $ErSi_9^-$, and $ErSi_{10}^-$ prefers to take part in bonding. That is, $ErSi_n$ clusters belong to AB type. The total magnetic moments of $ErSi_n$ and their anions are mainly provided by the 4*f* electrons of Er atom.

Acknowledgements This study was supported by the National Natural Science Foundation of China (Grant No. 21263010), by Program for Innovative Research Team in Universities of Inner Mongolia Autonomous Region (Grant No. NMGIRT-A1603), and by the Inner Mongolia Natural Science Foundation (Grant No. 2015MS0216).

References

1. A. J. Kenyon (2005). *Semicond. Sci. Technol.* **20**, R65–R84.
2. T. T. Cao, L. X. Zhao, X. J. Feng, Y. M. Lei, and Y. H. Luo (2009). *J. Mol. Struct. THEOCHEM* **895**, 148–155.
3. S. He and J. C. Yang (2017). *J. Clust. Sci.* **28**, 2309–2322.
4. R. N. Zhao, Z. Y. Ren, P. Guo, J. T. Bai, C. H. Zhang, and J. G. Han (2006). *J. Phys. Chem. A* **110**, 4071–4079.
5. R. N. Zhao, J. G. Han, J. T. Bai, F. Y. Liu, and L. S. Sheng (2010). *Chem. Phys.* **372**, 89–95.
6. R. N. Zhao, J. G. Han, J. T. Bai, and L. S. Sheng (2010). *Chem. Phys.* **378**, 82–87.
7. X. H. Xie, D. S. Hao, and J. C. Yang (2015). *Chem. Phys.* **461**, 11–19.
8. T. G. Liu, W. Q. Zhang, and Y. L. Li (2014). *Front. Phys.* **9**, 210–218.
9. L. Y. Hou, J. C. Yang, and Y. M. Liu (2016). *J. Mol. Model.* **22**, 193.
10. R. N. Zhao and J. G. Han (2014). *RSC Adv.* **4**, 64410–64418.
11. L. Y. Hou, J. C. Yang, and Y. M. Liu (2017). *J. Mol. Model.* **23**, 117.
12. Y. Z. Bai, G. F. Zhao, X. F. Shen, J. M. Sun, and Y. X. Wang (2011). *Acta Phys. Chim. Sin.* **27**, 39–46.
13. T. G. Liu, G. F. Zhao, and Y. X. Wang (2011). *Phys. Lett. A* **375**, 1120–1127.
14. J. C. Yang, Y. T. Feng, X. H. Xie, H. W. Wu, and Y. M. Liu (2016). *Theor. Chem. Acc.* **135**, 204.
15. G. F. Zhao, J. M. Sun, Y. Z. Gu, and Y. X. Wang (2009). *J. Chem. Phys.* **131**, 114312.
16. J. C. Yang, J. Wang, and Y. R. Hao (2015). *Theor. Chem. Acc.* **134**, 81.
17. C. G. Li, L. J. Pan, P. Shao, L. P. Ding, H. T. Feng, D. B. Luo, and B. Liu (2015). *Theor. Chem. Acc.* **134**, 34.
18. X. H. Xie, D. S. Hao, Y. M. Liu, and J. C. Yang (2015). *Comput. Theor. Chem.* **1074**, 1–8.
19. Y. T. Feng, J. C. Yang, and Y. M. Liu (2016). *Theor. Chem. Acc.* **135**, 258.
20. Y. T. Feng and J. C. Yang (2017). *J. Mol. Model.* **23**, 180.
21. Q. Peng and J. Shen (2008). *J. Chem. Phys.* **128**, 084711.
22. T. T. Cao, X. J. Feng, L. X. Zhao, X. Liang, Y. M. Lei, and Y. H. Luo (2008). *Eur. Phys. J. D* **49**, 343–351.
23. S. Jaiswal, V. P. Babar, and V. Kumar (2013). *Phys. Rev. B* **88**, 085412.
24. J. Lu, J. C. Yang, Y. I. Kang, and H. M. Ning (2014). *J. Mol. Model.* **20**, 2114.
25. N. Borshch and S. Kurganskii (2014). *J. Appl. Phys.* **116**, 124302.
26. A. Grubisic, H. P. Wang, Y. J. Ko, and K. H. Bowen (2008). *J. Chem. Phys.* **129**, 054302.
27. A. Grubisic, Y. J. Ko, H. P. Wang, and K. H. Bowen (2009). *J. Am. Chem. Soc.* **131**, 10783–10790.
28. M. Ohara, K. Miyajima, A. Pramann, A. Nakajima, and K. Kaya (2002). *J. Phys. Chem. A* **106**, 3702–3705.
29. K. Koyasu, J. Atobe, S. Furuse, and A. Nakajima (2008). *J. Chem. Phys.* **129**, 214301.
30. V. Kumar, A. K. Singh, and Y. Kawazoe (2006). *Phys. Rev. B* **74**, 125411.
31. J. P. Perdew, K. Burke, and M. Ernzerhof (1996). *Phys. Rev. Lett.* **77**, 3865–3868.
32. V. N. Staroverov, G. E. Scuseria, J. Tao, and J. P. Perdew (2003). *J. Chem. Phys.* **119**, 12129–12137.

33. A. D. Becke (1993). *J. Chem. Phys.* **98**, 5648–5652.
34. C. Lee, W. Yang, and R. G. Parr (1988). *Phys. Rev. B* **37**, 785–789.
35. D. E. Woon and T. H. Dunning Jr. (1993). *J. Chem. Phys.* **98**, 1358–1371.
36. X. Y. Cao and M. Dolg (2002). *J. Mol. Struct. THEOCHEM* **581**, 139–147.
37. A. A. Buchachenko, G. Chałasiński, and M. M. Szczęśniak (2007). *Struct. Chem.* **18**, 769–772.
38. M. J. Frisch, G. W. Trucks, H. B. Schlegel, G. E. Scuseria, M. A. Robb, J. R. Cheeseman, G. Scalmani, V. Barone, B. Mennucci, G. A. Petersson, H. Nakatsuji, M. Caricato, X. Li, H. P. Hratchian, A. F. Izmaylov, J. Bloino, G. Zheng, J. L. Sonnenberg, M. Hada, M. Ehara, K. Toyota, R. Fukuda, J. Hasegawa, M. Ishida, T. Nakajima, Y. Honda, O. Kitao, H. Nakai, T. Vreven, J. A. Montgomery Jr., J. E. Peralta, F. Ogliaro, M. Bearpark, J. J. Heyd, E. Brothers, K. N. Kudin, V. N. Staroverov, T. Keith, R. Kobayashi, J. Normand, K. Raghavachari, A. Rendell, J. C. Burant, S. S. Iyengar, J. Tomasi, M. Cossi, N. Rega, J. M. Millam, M. Klene, J. E. Knox, J. B. Cross, V. Bakken, C. Adamo, J. Jaramillo, R. Gomperts, R. E. Stratmann, O. Yazyev, A. J. Austin, R. Cammi, C. Pomelli, J. W. Ochterski, R. L. Martin, K. Morokuma, V. G. Zakrzewski, G. A. Voth, P. Salvador, J. J. Dannenberg, S. Dapprich, A. D. Daniels, O. Farkas, J. B. Foresman, J. V. Ortiz, J. Cioslowski, and D. J. Fox *Gaussian 09, Revision C.01* (Gaussian Inc., Wallingford CT, 2010).
39. J. Zhang and M. Dolg (2015). *Phys. Chem. Chem. Phys.* **17**, 24173–24181.
40. M. Dolg, H. Stoll, A. Savin, and H. Preuss (1989). *Theor. Chim. Acta.* **75**, 173–194.
41. J. C. Yang, W. G. Xu, and W. S. Xiao (2005). *J. Mol. Struct. THEOCHEM* **719**, 89–102.
42. Xl Zhu and X. C. Zeng (2003). *J. Chem. Phys.* **118**, 3557–3570.
43. E. J. Baerends, O. V. Gritsenkoab, and R. V. Meer (2013). *Phys. Chem. Chem. Phys.* **15**, 16408–16425.